PHYSICAL REVIEW A **74**, 011601(R) (2006)

Finite-temperature momentum distribution of a trapped Fermi gas

Qijin Chen,[1] C. A. Regal,[2] D. S. Jin,[2] and K. Levin[1]
[1]*James Franck Institute and Department of Physics, University of Chicago, Chicago, Illinois 60637, USA*
[2]*JILA, Quantum Physics Division National Institute of Standards and Technology and University of Colorado and Department of Physics, University of Colorado, Boulder, Colorado 80309-0440, USA*
(Received 20 April 2006; published 13 July 2006)

We present measurements of the temperature-dependent momentum distribution of a trapped Fermi gas consisting of ^{40}K in the BCS to Bose-Einstein condensation crossover regime. Accompanying theoretical results based upon a simple mean-field ground state are compared to the experimental data. Nonmonotonic effects associated with temperature T arise from the competition between thermal broadening and a narrowing of the distribution induced by the decrease in the excitation gap $\Delta(T)$ with increasing T.

DOI: 10.1103/PhysRevA.74.011601 PACS number(s): 03.75.Hh, 03.75.Ss, 74.20.−z

The recent discovery of superfluidity in trapped fermionic gases has paved the way for arriving at a much deeper understanding of the phenomena of superfluidity and superconductivity [1–8]. This may ultimately have application in high-temperature (T) superconductors [9,10], nuclear, astro-, and particle physics. In these trapped gases one has the ability to tune the strength of the attractive interaction that leads to pairs of fermions (Cooper pairs), which then Bose condense. As the pairing strength is increased a smooth crossover from BCS behavior to Bose-Einstein condensation (BEC) occurs. This tunability is a remarkable feature of trapped atomic gases and arises from a phenomenon known as a Feshbach resonance. In general the resulting superfluid state is more complex than that of simple BCS theory. Similarly the normal state is expected to be quite different from its BCS analog, since in general pairing takes place at higher temperatures (T^*) than the condensation temperature (T_c).

The ultracold gases have, thus, presented us with an opportunity to investigate in a more complete fashion all aspects of fermionic superfluidity. Because of their charge neutrality and trap confinement effects there exists a different set of tools for their experimental investigation, among which are measurements of the real space and momentum space distributions of the atomic fermions [11–15]. At finite T these distributions must change significantly in ways that reflect both pairing and possibly the onset of phase coherence.

In this paper we study both experimentally and theoretically the T dependence of the momentum distribution of fermionic atoms within a trapped Fermi gas. Recent measurements of this momentum distribution near $T=0$ showed a dramatic broadening as the pairing strength increased [13], as is qualitatively consistent with theoretical calculations [13,16]. In the present paper we extend these measurements by varying T from below to well above the theoretically predicted values of T_c; this allows us to probe the momentum distribution in the normal as well as the superfluid phase.

In general, in a $T=0$ fermionic system the physical phenomenon that controls the momentum distribution is pairing. In the BCS theory the momentum distribution of a homogeneous sample shows a slight smearing of the Fermi surface due to pairing. This effect is very small and associated with the gap parameter Δ. In the BCS-BEC crossover, however, one greatly increases the interaction strength that leads to pairing. It is conventional to parametrize the state within this crossover in terms of $k_F^0 a$, where a is the two-body s-wave scattering length between atoms and k_F^0 is the Fermi wave vector in the noninteracting limit. While in the BCS limit ($1/k_F^0 a \to -\infty$) it is difficult to observe the slight change in the momentum distribution, as the interaction strength increases this broadening grows. Indeed, at unitarity ($1/k_F^0 a = 0$) the broadening is no longer small, but instead comparable to the Fermi energy. Finally, in the BEC limit ($1/k_F^0 a \to \infty$) the atomic momentum distribution becomes extremely broad and corresponds to the square of the molecular wave function in momentum space.

At finite T one expects a similar broadening of the momentum distribution as the interaction is increased. However, the extent of this broadening is determined by the T dependence of the excitation gap $\Delta(T)$; it is maximum at $T=0$ and should disappear as $\Delta(T)$ goes to zero around T^*, where all pairs are broken. This effect of pairing on the distribution will occur in addition to the usual thermal broadening of the momentum profile that occurs in a Fermi gas. While the thermal broadening increases with T, the pairing induced broadening decreases with T. As we will show below, these two competing effects lead to a nontrivial T dependence in the Fermi gas momentum distribution.

While the discussion thus far has centered on the expectation for a homogeneous Fermi gas, the experiments presented here take place in a harmonic trapping potential. The local Fermi wave vector in a trap varies with position r, so that the integrated momentum distribution for a noninteracting Fermi gas is significantly different from that for a homogeneous case [13]. Thus, in addition to the local broadening due to pairing, the trapping potential compresses the density profile and thereby enlarges the overall momentum distribution.

To perform our experiments, we follow the techniques described in Refs. [17,18] to create an ultracold ^{40}K gas. Briefly, starting with a cold gas we slowly ramp a magnetic field to approach a wide Feshbach resonance at 202.1 ± 0.1 G [3]. The rate of the field ramp $(6.5\ \mathrm{ms/G})^{-1}$ is slow enough to ensure adiabaticity with respect to many-body time scales in the system. We then probe the momentum distribution of atoms in this final state using the experimental sequence developed in Ref. [13]. In this sequence the atom gas must

expand freely without any interatomic interactions; this we achieve through a fast magnetic-field ramp (here $\approx 8\ \mu$s/G) to $a \approx 0$ [11]. This is followed by the standard technique of time-of-flight expansion and optical absorption imaging.

To obtain the data in this paper we repeat the process above for gases at a variety of interaction strengths and at a variety of temperatures. To vary the temperature of our initial Fermi gas we increase the depth of our optical dipole trap after evaporative cooling and heat the gas by modulating the optical trap strength. To characterize the temperature of the gas we measure the temperature compared to the Fermi temperature in the noninteracting limit $(T/T_F)^0$. The physical T at a given $k_F^0 a$ can then be extracted using the theoretical thermometry described in Ref. [19], which is based upon entropy conservation in the adiabatic magnetic-field ramp.

In Fig. 1, we plot experimental azimuthally averaged momentum distributions as a function of k/k_F^0. From top to bottom, each panel corresponds to a fixed $(T/T_F)^0 = 0.11$, 0.2, 0.3, 0.5, 0.7, and 1.0, with variable $1/k_F^0 a$. The scattering strength $1/k_F^0 a = -71$, -0.5, 0.0, and 0.5 represent the noninteracting Fermi gas, near-BCS, unitary, and near-BEC cases, respectively. For each set of measured distributions at a particular $(T/T_F)^0$, parameters such as trap strength and initial gas density are fixed. However, these parameters vary among the different sets at constant $(T/T_F)^0$ (panels in Fig. 1). For example, for the data at $(T/T_F)^0 = 0.11$ the peak density, for atoms in one spin state, in the weakly interacting regime is $n_{pk}^0 = 1.4 \times 10^{13}$ cm^{-3} and $E_F^0 = 0.56\ \mu$K. For the hottest data n_{pk}^0 decreases to 6×10^{12} cm^{-3} and $E_F^0 = 0.79\ \mu$K.

On top of the data points in Fig. 1 we show a fit to an empirical function, which we utilize both for normalization and for later data analysis. We apply the following two-dimensional (2D) surface fit to the measured optical depth D of the expanded Fermi gas.

$$D(x,y) = D_{pk} g_2(-\zeta e^{-x^2/2\sigma_x^2 - y^2/2\sigma_y^2})/g_2(-\zeta), \qquad (1)$$

Here $g_n(x) = -\frac{1}{\Gamma(n)} \int_0^\infty d\epsilon \frac{\epsilon^{n-1}}{1 - e^{\epsilon}/x} = \Sigma_{l=1}^{\infty} \frac{x^l}{l^n}$ is the polylogarithmic function, ζ is the fugacity, and $\sigma_{x,y}^2$ are proportional to the Fermi gas temperature and related to the expansion time t. This form can be derived microscopically in the limit of weak interactions, where $\zeta \to e^{\mu/k_B T}$. While this equation is only physically valid for an ideal Fermi gas, empirically we find that it fits reasonably well to the data throughout the crossover [13]. In this way the 2D momentum distribution is given by $N_{2D}(k_x, k_y) = AD(\hbar k_x t/m, \hbar k_y t/m)$. Here A is a normalization constant such that $\int \frac{d^2k}{(2\pi)^2} N_{2D}(k_x, k_y) = N_a$, where N_a is the total number of atoms.

The experimental results of Fig. 1 show that, at $(T/T_F)^0 = 0.11$, as the system passes from an ideal Fermi gas to near-BEC the momentum distribution widens significantly, just as in the $T=0$ case shown in Ref. [13]. As $(T/T_F)^0$ increases the effect of pairing becomes less pronounced, and at sufficiently high T the curves coalesce. Here $\Delta(T) \ll T$, and the system basically behaves as a classical gas of atoms.

Theoretical calculations for the momentum distributions in the crossover are presented in the right column of Fig. 1. The calculations are based on a generalized mean-field

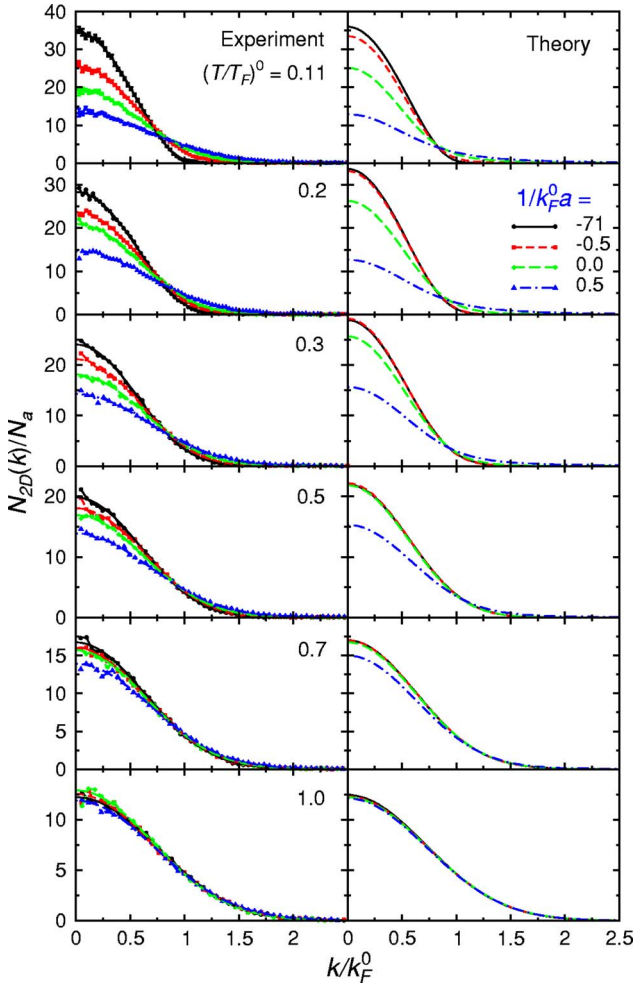

FIG. 1. (Color online) Evolution of the momentum distribution $N_{2D}(k)$ with the interaction strength $1/k_F^0 a$ from noninteracting to near-BEC cases. The two columns compare experiment (left) and theory (right). Different rows correspond to different values of $(T/T_F)^0$. The lines in the experimental plots correspond to a fit to Eq. (1). The value of k_F^0 used to create the experimental plots was determined through experimental measurements of the particle number and trap strength, which led to systematic uncertainties in k_F^0 of up to 10% for these data. While the raw data are shown here, the normalization applied in Fig. 3 removes this systematic error.

theory [9,20], which is consistent with the BCS-Leggett ground state [21]. While $T=0$ momentum profiles of this state have been discussed in the literature [13,16], here we include finite T effects. An important aspect of this theory is that the fermionic excitation gap $\Delta(T)$ becomes distinct from the superfluid order parameter $\Delta_{sc}(T)$ at finite T (except in the strict BCS regime). This point is illustrated in Fig. 2(a). Here the trap-averaged value of the excitation gap, $\langle \Delta^2 \rangle^{1/2}$, is shown as a function of $(T/T_F)^0$ for the near-BEC $(1/k_F^0 a = 0.5)$, unitary $(1/k_F^0 a = 0)$, and near-BCS $(1/k_F^0 a = -0.5)$ cases from top to bottom. The arrows indicate the calculated value of T_c^0. We find that $\Delta(T)$ has a gentle onset at high T, corresponding to the pair formation temperature T^*, which is generally much higher than T_c.

The momentum and density distribution, along with the chemical potential μ, the gap parameter, and the order pa-

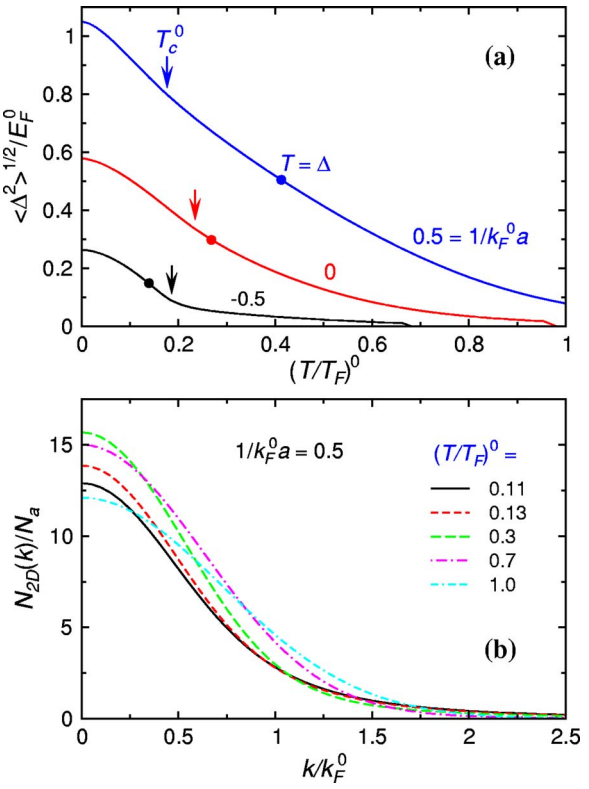

FIG. 2. (Color online) (a) Temperature dependence of the average excitation gap $\langle\Delta^2\rangle^{1/2}$ at $1/k_F^0 a=0.5$ [top (blue) curve], 0 [middle (red) curve], and −0.5 [bottom (black) curve]. The solid circles indicate where this effective gap coincides with the temperature. The arrows indicate the transition temperatures T_c^0. (b) Theoretical momentum distributions $N_{2D}(k)$ at a variety of temperatures for $1/k_F^0 a=0.5$.

rameter, are self-consistently determined using the local density approximation. The local momentum distribution is given by

$$n_k(r) = 2\{v_{\mathbf{k}}^2[1 - f(E_{\mathbf{k}})] + u_{\mathbf{k}}^2 f(E_{\mathbf{k}})\}, \tag{2}$$

where $u_{\mathbf{k}}^2, v_{\mathbf{k}}^2 = \{1 \pm [\epsilon_{\mathbf{k}} - \mu(r)]/E_{\mathbf{k}}(r)\}/2$ are the BCS coherence factors; $\epsilon_{\mathbf{k}} = \hbar^2 k^2/2m$ is the kinetic energy of free fermions, $E_{\mathbf{k}} = \sqrt{[\epsilon_{\mathbf{k}} - \mu(r)]^2 + \Delta^2}$ the fermionic quasiparticle dispersion, and $f(x)$ the Fermi-Dirac distribution function. Then the trap-integrated momentum distribution $N(k)$ and its 2D projection are given, respectively, by

$$N(k) = \int d^3 r n_k(r) \text{ and } N_{2D}(k) = \int \frac{dk_z}{2\pi} N(k). \tag{3}$$

Note, it is $N_{2D}(k)$ that is directly comparable with our experimentally measured optical depth. It can be seen that the effects of superfluidity and of pairing more generally enter only through $E_{\mathbf{k}}$ which, in turn, depends upon $\Delta(T)$. Thus the momentum distribution represents, in effect, the behavior of the excitation gap, not the order parameter Δ_{sc}. Details of the theoretical formalism can be found in Ref. [9].

Near $T=0$ it has been shown that the simple mean-field ground state we use here semi-quantitatively describes the momentum distribution and effective kinetic energy [13,22]. Thus, this ground state is an excellent starting point for finite-T comparisons between theory and experiment. Quantitatively, weaknesses of the mean-field ground state in reproducing the momentum distribution exist, as seen in Ref. [22]. These weaknesses include that, in the BEC regime, the interboson scattering length is overestimated by roughly a factor of 3. However, this does not substantially affect the momentum distribution of atoms we address, in part because for the $k_F^0 a$ considered here we confine our attention to the fermionic regime ($\mu > 0$). [For $1/k_F^0 a=0.5$, our calculation shows $\mu(r=0)/E_F^0=0.23$ at T_c.] Second, the theory does not include the Hartree self-energy. We also do not take into account the finite rate of the magnetic-field ramp above the Feshbach resonance as was done theoretically in Ref. [13]. This finite ramp rate leads to slight redistribution of the momentum so that high-energy spectral weight is somewhat suppressed. This effect is crucial for accurately comparing to the effective kinetic energy [13,22], but for our ramp rates and in the fermionic regime we expect the effect on our distribution comparisons to be small.

We now focus on the comparison between our mean-field calculations and the experiment shown in Fig. 1. Overall we find semiquantitative agreement. However, there are discrepancies that can be seen in the profiles, especially in the middle range of $1/k_F^0 a$. This can be attributed mainly to the neglect of the Hartree term in the theoretical formalism that was noted above. If we were to include the Hartree correlation, our calculation of the chemical potential μ would decrease; this would result in a wider spread between the noninteracting and interacting profiles in the theoretical portion of Fig. 1 and, thus, a better quantitative agreement with experiment.

We now turn to understanding the T dependence of the distribution at a fixed value of $1/k_F^0 a$. In this analysis one expects a competition between conventional thermal broadening and narrowing due to the decrease of $\Delta(T)$ with increasing T. To illustrate this quantitatively we turn to Fig. 2(a). The solid circles indicate where the effective gap coincides with the temperature. This corresponds roughly to the temperature at which the broadening as a function of T should display an inflection point.

In Fig. 2(b) we plot the theoretical results for the momentum distribution at a fixed $1/k_F^0 a=0.5$. Indeed, there is a change in the T dependence of the curves that occurs roughly when $\langle\Delta^2\rangle^{1/2} = k_B T$. Below this temperature, the behavior of the distribution tends to be dominated by that of Δ, and the distribution initially narrows with increasing T. Above this temperature, thermal effects dominate and the distribution widens with increasing T. We find analogous nonmonotonic behavior at the unitary limit.

To test this theoretical prediction of a nonmonotonic T dependence of the broadening, we plot the half width (HW) at half height of the distributions as a function of $(T/T_F)^0$. The experimental HW is determined from a fit of the data to Eq. (1) using the curves in Fig. 1 as well as additional similar data. For this analysis we have eliminated the dominant uncertainty associated with the determination of E_F^0 (and hence k_F^0) by applying a multiplicative correction factor; this factor is simply the ratio of the calculated and measured half-

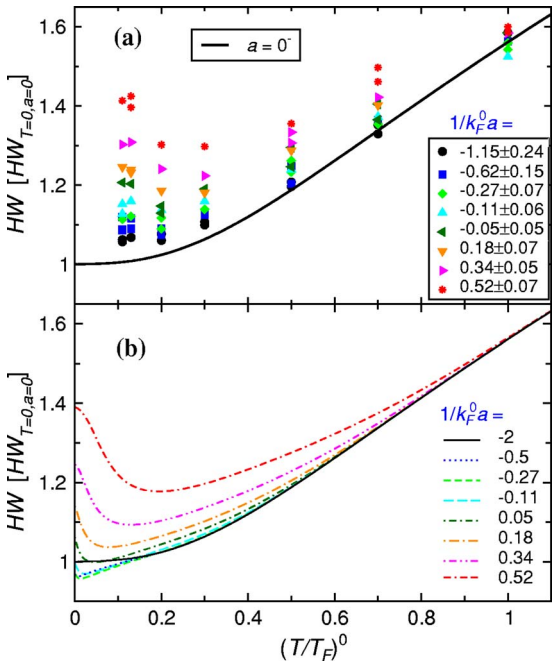

FIG. 3. (Color online) Comparison of the half width (HW) at half height as a function of $(T/T_F)^0$ for different values of $1/k_F^0 a$ from the noninteracting (bottom curve) to near-BEC (top curve) cases between (a) experiment and (b) theory. The HW in the experimental case is normalized to eliminate dependence upon the experimental determination of E_F^0 (see text); this results in perfect agreement with theory in the noninteracting case [solid (black) line].

widths for the weakly interacting limit. This is done for each set of data taken at fixed $(T/T_F)^0$.

Figure 3(a) shows the experimental results; the different symbols represent groups of data with an average value of $1/k_F^0 a$ indicated by the legend. The black line represents the theoretical dependence of the HW in the noninteracting ($a=0$) limit. As expected for this limit, in the classical regime the width scales linearly with T; the width then levels out to a finite value due to Pauli pressure. As the interaction is increased [(black) circles to (red) stars] the decrease of the width with decreasing T becomes less dramatic, and at the lowest T the width actually begins to increase as a function of T. This temperature nonmonotonicity is particularly apparent on the BEC side of the Feshbach resonance.

The experimental result of Fig. 3(a) compares favorably with its theoretical counterpart [Fig. 3(b)] in that they both display nonmonotonic T dependence. Note that the theoretical HW at low T and weak interaction is smaller than its experimental counterpart; in this regime the width drops below the noninteracting curve due to the absence of the Hartree term and changes in the shape of the distribution. This aspect of the theory result again accentuates that, while we have found the simple mean-field theory to be an excellent starting point for finite-temperature studies, future quantitative studies will require theories that incorporate the Hartree term.

In summary, we have studied the momentum distribution of trapped fermionic atoms at finite T by a detailed comparison of theory and experiment. Our results show that there is a competition between the T dependence of the fermionic excitation gap and thermal broadening, which leads to nonmonotonicities in the T dependence of the momentum profiles. Since temperature is often difficult to determine experimentally, systematic studies at nonzero T are just beginning in these ultracold gases. Here, by working with a theoretical temperature scale (set by the entropy), under conditions of an adiabatic sweep, we are able to show semiquantitative agreement between theory and experiment using a simple mean-field theory.

We thank Cheng Chin for helpful comments. This work was supported by NSF, NASA, and NSF-MRSEC Grant No. DMR-0213745. C.A.R. acknowledges support from the Hertz Foundation.

[1] M. Greiner, C. A. Regal, and D. S. Jin, Nature (London) **426**, 537 (2003).
[2] S. Jochim *et al.*, Science **302**, 2101 (2003).
[3] C. A. Regal, M. Greiner, and D. S. Jin, Phys. Rev. Lett. **92**, 040403 (2004).
[4] M. W. Zwierlein *et al.*, Nature (London) **435**, 1047 (2005).
[5] J. Kinast *et al.*, Phys. Rev. Lett. **92**, 150402 (2004).
[6] M. Bartenstein *et al.*, Phys. Rev. Lett. **92**, 203201 (2004).
[7] J. Kinast, A. Turlapov, J. E. Thomas, Q. J. Chen, J. Stajic, and K. Levin,Science **307**, 1296 (2005).
[8] M. W. Zwierlein *et al.*, Phys. Rev. Lett. **92**, 120403 (2004).
[9] Q. J. Chen, J. Stajic, S. N. Tan and K. Levin, Phys. Rep. **412**, 1 (2005).
[10] Q. J. Chen, J. Stajic, and K. Levin, Low Temp. Phys. **32**, 406 (2006) [Fiz. Nizk. Temp. **32**, 538 (2006)].
[11] T. Bourdel *et al.*, Phys. Rev. Lett. **91**, 020402 (2003).
[12] M. Bartenstein *et al.*, Phys. Rev. Lett. **92**, 120401 (2004).
[13] C. A. Regal, M. Greiner, S. Giorgini, M. Holland, and D. S. Jin,Phys. Rev. Lett. **95**, 250404 (2005).
[14] G. B. Partridge *et al.*, Science **311**, 503 (2006).
[15] M. W. Zwierlein *et al.*, Science **311**, 5760 (2006).
[16] L. Viverit *et al.*, Phys. Rev. A **69**, 013607 (2004).
[17] C. A. Regal and D. S. Jin, Phys. Rev. Lett. **90**, 230404 (2003).
[18] B. DeMarco and D. S. Jin, Science **285**, 1703 (1999).
[19] Q. J. Chen, J. Stajic, and K. Levin, Phys. Rev. Lett. **95**, 260405 (2005).
[20] J. Stajic, Q. J. Chen, and K. Levin, Phys. Rev. Lett. **94**, 060401 (2005).
[21] A. J. Leggett, in *Modern Trends in the Theory of Condensed Matter* (Springer-Verlag, Berlin, 1980), pp. 13–27.
[22] M. L. Chiofalo, S. Giorgini, and M. Holland, e-print cond-mat/0512460.